Toxicology and Applied Pharmacology 449 (2022) 116130

Contents lists available at ScienceDirect

Toxicology and Applied Pharmacology

journal homepage: www.elsevier.com/locate/taap

Paracetamol perturbs neuronal arborization and disrupts the cytoskeletal proteins SPTBN1 and TUBB3 in both human and chicken in vitro models

Nils-Anders Labba [a,b,c], Hallvard Austin Wæhler [b,c], Nora Houdaifi [a], Denis Zosen [a], Fred Haugen [d], Ragnhild Elisabeth Paulsen [a,c], Mussie Ghezu Hadera [a,c], Ragnhild Eskeland [b,c,*]

[a] Section for Pharmacology and Pharmaceutical Biosciences, Department of Pharmacy, Faculty of Mathematics and Natural Sciences, University of Oslo, Norway
[b] Department of Molecular Medicine, Institute of Basic Medical Sciences, Faculty of Medicine, University of Oslo, Norway
[c] PharmaTox Strategic Research Initiative, Faculty of Mathematics and Natural Sciences, University of Oslo, Norway
[d] Department of Work Psychology and Physiology, National Institute of Occupational Health (STAMI), Oslo, Norway

ARTICLE INFO

Editor: Lawrence Lash

Keywords:
Neurodevelopmental toxicology
APAP
Cerebellar granule neurons
NTERA2
Cell viability
Neuritogenesis
β2-spectrin
β3-tubulin

ABSTRACT

Epidemiological studies have linked long-term/high-dose usage of paracetamol (*N*-acetyl-para-aminophenol, APAP) during pregnancy to adverse neuropsychiatric outcomes, primarily attention-deficit hyperactive disorder (ADHD), in the offspring. Though variable, ADHD has been associated with phenotypic alterations characterized by reductions in grey matter densities and aberrations in structural connectivity, effects which are thought to originate in neurodevelopment. We used embryonic chicken cerebellar granule neurons (CGNs) and neuronally differentiating human NTERA2 cells (NT2Ns) to investigate the in vitro effects of APAP on cell viability, migration, neuritogenesis, and the intracellular levels of various proteins involved in neurodevelopment as well as in the maintenance of the structure and function of neurites. Exposure to APAP ranging from 100 to 1600 μM yielded concentration- and time-dependent reductions in cell viability and levels of neurite arborization, as well as reductions in the levels of the cytoskeletal protein β2-spectrin, with the highest APAP concentration resulting in between 50 and 75% reductions in the aforementioned metrics over the course of 72 h. Exposure to APAP also reduced migration in the NT2Ns but not CGNs. Moreover, we found concentration- and time-dependent increases in punctate aggregation of the cytoskeletal protein β3-tubulin following exposure to APAP in both cell model systems, with the highest APAP concentration approximately doubling the number of aggregates over 72–120 h. Our findings demonstrate that APAP negatively perturbs neurite arborization degree, with concurrent reductions in the protein levels of β2-spectrin and disruption of the integrity of β3-tubulin, both proteins of which play important roles in neuronal structure and function.

1. Introduction

The World Health Organization has estimated that neuropsychiatric disorders are among the largest contributors of disease burden of non-communicable conditions globally for children under the age of 15 irrespective of socioeconomic status, accounting for 8% of deaths and one third of disability-adjusted life years (World Health Organization, 2008). Neuropsychiatric disorders are among the paradigmatic examples of ailments with multifactorial aetiologies, with underlying genetic predispositions, epigenetic factors, and exposure to xenobiotics all contributing to the manifestation of these disorders (De Felice et al., 2015; Bakulski et al., 2016). The development of the nervous system is comprised of an intricately choreographed series of spatiotemporally interrelated events (proliferation, migration, differentiation, synaptogenesis, gliogenesis, myelination, and apoptosis), the perturbation of any of which can result in permanent abnormality (Sachana et al., 2019). Attention-deficit hyperactivity disorder (ADHD) is one of the most widespread neuropsychiatric disorders of neurodevelopmental origin, and despite being considered highly multifactorial, is often associated with reductions in volume of both general grey matter and white matter densities (Martine Hoogman, 2017; Mostofsky et al., 2002). Additionally, differential reductions in specific brain regions (Carmona et al., 2005), and perturbations of structural connectivity both at the level of circuits and at the level of brain regions have also been

* Corresponding author at: Division of Biochemistry, Institute of Basic Medical Sciences, Dep. of Molecular Medicine, University of Oslo, PO Box 1112, Blindern, 0317 Oslo, Norway.
E-mail address: ragnhild.eskeland@medisin.uio.no (R. Eskeland).

https://doi.org/10.1016/j.taap.2022.116130
Received 7 January 2022; Received in revised form 28 May 2022; Accepted 10 June 2022
Available online 15 June 2022

reported (Beare et al., 2017; Sidlauskaite et al., 2015).

Paracetamol (*N*-acetyl-para-aminophenol, APAP) is the most commonly used over-the-counter analgesic, and is the first-in-line recommendation for use in pregnancy due to its established lack of teratogenic effects (McElhatton et al., 1997). However, recent large-scale epidemiological investigations have found associations between heavy and/or long-term use of APAP during pregnancy and the development of negative neuropsychiatric outcomes in the offspring, primarily ADHD (Brandlistuen et al., 2013; Ystrom et al., 2017; Liew et al., 2014; Ji et al., 2020; Stergiakouli et al., 2016; Thompson et al., 2014; Tovo-Rodrigues et al., 2018). APAP distributes homogeneously (Forrest et al., 1982) and permeates both the placental barrier (Nitsche et al., 2017) and the blood-brain barrier (Bannwarth et al., 1992; Anderson et al., 1998; Kumpulainen et al., 2007), with peripartal plasma samplings showing equimolar concentrations in mother and child (Nitsche et al., 2017). The physiological half-life of APAP has been estimated to range between 2 and 4 h (Schiødt et al., 2002), with hepatic dysfunction increasing clearance time considerably (Froomes et al., 1999). APAP and its metabolites are known to interact with a variety of systems considered crucial to early neurodevelopment, including constituents of the monoaminergic systems (de Fays et al., 2015; Blecharz-Klin et al., 2017; Blecharz-Klin et al., 2015a; Blecharz-Klin et al., 2015b; Blecharz-Klin et al., 2019), the endocannabinoid system (Schultz et al., 2021), and the expression of brain-derived neurotrophic factor (Blecharz-Klin et al., 2018; Viberg et al., 2014). Recently APAP has also been found to induce proteolytic breakdown of β2-spectrin, or spectrin beta non-erythrocytic 1 (SPTBN1) in hepatocytes (Baek et al., 2016). SPTBN1, canonically considered a scaffolding protein that stabilizes the actin cytoskeleton (Machnicka et al., 2014), has in the last decade been found to be implicated in a multitudinous set of neuronal functions including adhesion (Tian et al., 2012), neuritogenesis (Tian et al., 2012; Zhong et al., 2014; Xu et al., 2013; Lee et al., 2012), axonal transport (Lorenzo et al., 2019), myelination (Susuki et al., 2011), synaptic stabilization (Sikorski et al., 2000) and signaling (Sikorski et al., 2000). Mutations in SPTBN1 in patients have been associated with a variety of neuropsychiatric abnormalities related to neurodevelopment (Cousin et al., 2021), in addition to SPTBN1 being a top hit among ADHD-associated protein truncating variants (Satterstrom et al., 2019). Despite its wide range of interactions, short-term exposure to APAP at therapeutic doses exhibits low cytotoxicity in various types of in vitro neuronal culture models (Xie and Harvey, 1993; Mannerström et al., 2006; Tripathy and Grammas, 2009; Schultz et al., 2012; Posadas et al., 2010; Oksuz et al., 2021), and is widely regarded as a safe medication for use during pregnancy (Toda, 2017).

Neuritogenesis is a highly sensitive developmental process that gives rise to the dendritic and axonal processes that form the basis for the structural connectivity of the central nervous system (Mueller et al., 2000), and which is recapitulated by neuronally differentiating cells in vitro. In this work, we employed cell culture of embryonic chicken cerebellar granule neurons (CGNs) to investigate the effects of APAP on cell viability and neuritogenesis. Chicken CGNs constitute an easily accessible and 3R's compliant source for highly homogenous neuronal culture which undergoes all key stages of early neurodevelopment, including neuritogenesis (Bjørnstad et al., 2015). Moreover, as ADHD has been associated with perturbations in cerebellar structure and function, favours CGNs as a biological relevant model system (Stoodley, 2016; Kim et al., 2017). We also utilized the human NTERA2 embryo carcinoma cell line, which has previously been shown to undergo retinoic acid (RA)-mediated differentiation into neuronal cells exhibiting transcriptional expression patterns consistent with forebrain, hindbrain and spinal cord neurons. Neuronally differentiating NTERA2 cells (NT2Ns) progress through all stages of neurodevelopment, including neuritogenesis, terminating in post-mitotic cells exhibiting polarized neuronal morphology and expressing neuron-specific proteins of a wide variety (Pleasure et al., 1992). The NT2N culture has been validated as an appropriate human model for studies of developmental neurotoxic effects (Stern et al., 2014). Terminally differentiated NT2Ns have been used in xenografts in stroke victims in phase 1 and 2 clinical trials (Meltzer et al., 2001; Kondziolka et al., 2005), exhibiting no negative effects and in some cases being integrated into neuronal circuits (Nelson et al., 2002). We sought to investigate whether the extant literature findings on the putative cytotoxic and neurotoxic effects of APAP in various in vitro models could be recapitulated and expanded upon in an explicitly neurodevelopmental paradigm, and whether any observed toxicity metrics could be linked to the epidemiological findings correlated with peripartal exposure to APAP. In order to mimic a developmental exposure paradigm, we treated both the CGNs and the NT2Ns at pre-terminally differentiated stages corresponding to the transition between late neuroprogenitors and immature neurons. Given the importance of SPTBN1 for the development and maintenance of neurites, we hypothesized that if SPTBN1 was undergoing APAP-mediated breakdown, neurite arborization should be compromised as a result. We selected a range of physiologically relevant APAP concentrations between 25 μM and 1600 μM on the basis of reported plasma peak concentrations following oral administration of APAP in both therapeutic (100–200 μM) (Graham et al., 1999; Trettin et al., 2014) and hepatotoxic (≥800 μM) (Marks et al., 2017; Ye et al., 2018) concentrations, exposed CGNs and NT2Ns and assayed cell viability and neurite arborization, as well as the protein levels for proteins relevant for neurodevelopment.

2. Materials and methods

2.1. Laboratory animals and preparation of CGN primary culture

All procedures involving animals were approved by the Norwegian Animal Welfare Act (FOTS id 13,896) and performed in accordance with the EU Directive 2010/63/EU. We obtained fertilized eggs (*Gallus gallus*) from Nortura Samvirkekylling, Våler, Norway. We incubated the eggs at 37.5 °C, 45% humidity in an OvaEasy 380 Advance EXII Incubator (Brinsea, Weston-super-Mare, UK). On embryonic day 17, we performed hypothermic anaesthesia on *in ovo* embryos by submergence in crushed ice for 7 min prior to sacrifice and cerebellar excision. We pooled cerebella from 5 to 20 individual embryos into a buffered physiological solution consisting of 1× Krebs-Ringer solution with 3 g/L bovine serum albumin (BSA, Cytiva #SH30574.02) and 2.54 mM $MgSO_4$ and dissociated the cells mechanically using a scalpel followed by trituration via pipette. We washed the cells with additional physiological solution and centrifuged them at 200 RCF for 1 min, after which we trypsinized them in the previously mentioned physiological solution supplemented with 250 μg/mL trypsin (Sigma-Aldrich #T9201) for 15 min at 37 °C, with periodical agitation. We added four volumes of physiological solution supplemented with 95 μg/mL trypsin inhibitor (Sigma-Aldrich #T9003) and 22.5 μg/mL DNase I (Sigma-Aldrich #D5025) to halt the trypsinization process and centrifuged again at 200 RCF for 2 min. We discarded the supernatant and washed the cells with aforementioned physiological solution supplemented with $CaCl_2$ to a final concentration of 650 μM and with $MgSO_4$ adjusted to 2.82 mM, then we centrifuged the cells at 200 RCF for 7 min. Cells were resuspended in Basal Eagle's Medium (Gibco #41010–026) containing 7.5% heat-inactivated chicken serum (Gibco #16110082), 22 mM KCl, 2 mM Glutamine (Sigma-Aldrich #G8540), 100 nM insulin (Sigma-Aldrich #I5500), and 1% penicillin/streptomycin (ThermoFisher #15070063). Cells were seeded at a concentration of 530,000 cells/cm^2 into coated vessels (coating conditions were experiment-dependent and are specified below) and incubated at 37 °C, 5% CO_2 overnight. Treatment exposure was conducted using a defined medium composed of BME with 22 mM KCl, 2 mM Glutamine, 100 μg/mL holo-transferrin (Sigma-Aldrich, 616,397), 9.6 μg/mL putrescine (Sigma-Aldrich, P5780), 30 nM Na_2SeO_3 (Sigma-Aldrich, S5261), 1 nM T3 (Sigma-Aldrich #T6397), 25 μg/mL insulin, and 1% penicillin/streptomycin, and supplemented with 10 μM β-D-arabinofuranoside (AraC, Sigma-Aldrich #C1768) to limit glial proliferation.

For the MTT assays, we used Nunc™ MicroWell™ 96-Well Microplates (ThermoFischer #167008), whereas TPP® 96-well plates (Sigma-Aldrich #Z707910) were used in the live-cell imaging. In the immunocytochemical analyses, we used Corning® CellBIND® black-frame clear-bottom 96-well plates (Corning #3340). We coated all plastic vessels with 3 μg/cm^2 poly-L-lysine (PLL, Sigma-Aldrich # P9155) in MQ-water for 1 h at room temperature followed by aspiration of coating solution and drying of the substrate prior to cell seeding. For the immunocytochemical (ICC) analyses we used a second layer of coating consisting of Geltrex (ThermoFischer #A1413302) applied according to manufacturer's instructions in addition to the PLL-coating, and without allowing the PLL to dry prior to application of the second coating solution. Geltrex coating was not allowed to dry prior to the cell seeding. In the migration experiment we generated CGN spheroids by transferring 20 mL of serum-containing medium with DIV0 single-cell suspension at 2 × 10^6 cells/mL into 100 mm low-adhesion dishes, which we incubated overnight at 37 °C, 5% CO_2. On the following day, we dislodged and dissociated the cell clusters by very gently triturating 3–5 times with 25 mL serological pipette. We centrifuged the spheroids at 200 RCF for 30 s, resuspended them in 5 mL serum-containing medium, and centrifuged again at the same settings. After both centrifugation steps, we collected the supernatants containing single cells. We seeded the spheroids at a density of 1500 spheroids/cm^2 in serum-containing medium into PLL-coated TPP® 96-well plates (Sigma-Aldrich #Z707910). After seeding, we incubated the spheroids at 37 °C, 5% CO_2 for 4 h before exchanging serum-containing medium with AraC-containing defined medium with APAP treatment.

2.2. NTERA2 cell culture and preparation of NT2Ns

We cultured mycoplasma-tested human embryocarcinoma NTERA2 cells (ATCC #CRL-1973) at 37 °C with 5% CO_2 in maintenance medium composed of 10 mL high-glucose, GlutaMAX-containing Dulbecco's modified Eagle's medium (DMEM, Gibco #42430–025) supplemented with 10% fetal bovine serum (Capricorn Scientific #FBS-11A), 1 mM pyruvate (ThermoFischer #11360–070), and 1% penicillin/streptomycin (ThermoFischer #15140–122). We maintained the cells in 75 cm^2 plastic flasks (VWR #734–2313) that had been coated with 1.33 mg/cm^2 gelatin (Sigma-Aldrich #G1890-500G) in MQ-water for one hour at room temperature prior to removal of the coating solution, washing of vessels using PBS, and application of cell culture. We split the cells in a 1:10 ratio every 3 days at approximately 75% culture confluence by removal of medium, rinsing of cells with PBS, and incubation of cells in 2 mL trypsin (Gibco #25300054) at 37 °C with 5% CO_2 for 5 min prior to addition of 8 mL maintenance medium to halt trypsinization. We triturated the cells and replated 1 mL of the cell suspension while discarding the rest. To generate NT2Ns we modified a previously reported method for generating NT2Ns using agitated spheroid culture (Serra et al., 2007) to our convenience. We seeded 10 mL of NTERA2 cell suspension into 100 mm low-adhesion dishes at 5 × 10^5 cells/mL in maintenance medium and incubated at 37 °C with 5% CO_2 on a Celltron 69222 ø25mm rotator (Infors HT, Lonay, Switzerland) at 60 RPM for 2–4 days until spheroids formed. We collected and centrifuged the cell suspension at 200 RCF for 1 min and replaced the medium with fresh maintenance medium on a daily basis until the spheroids had grown to sizes visible to the naked eye. Once spheroids had formed, we initiated differentiation by replacing the medium with 10 mL maintenance medium supplemented with 10 μM all-trans retinoic acid (RA, ThermoFischer #R2625). For the first phase of differentiation (6 days in total), we performed half-volume medium changes every two days by removal of half of the total medium volume followed by addition of 5 mL fresh medium supplemented with 20 μM RA. On the sixth day we performed a half-volume medium removal, replacing the serum-containing maintenance medium with 5 mL defined medium composed of high-glucose, GlutaMAX-containing DMEM/12 (Gibco #31331–028) supplemented with 2% B27 (ThermoFischer #17504044) and 1% N2 (ThermoFischer #17502048), 1 mM pyruvate, 1% penicillin/streptomycin, and 20 μM RA. During this second phase of differentiation (14 days in total) in defined medium we again performed half-volume medium changes every two days, using defined medium instead of maintenance medium. We differentiated the NTERA2 cells into pre-terminal NT2N neurons in this suspended rotating spheroid format for a total of 20 days (excluding initial spheroid formation period in RA-free maintenance medium). Once 20 days had passed, we trypsinized and seeded the NT2Ns into PLL- and Geltrex-coated (as described in the section on CGN preparation) plastic vessels at 50.000 cells/cm^2 in a 1:1 mixture of conditioned and fresh defined medium, where the fresh half of the medium had been supplemented with 10 μM RA, and incubated at 37 °C, 5% CO_2 overnight for attachment. Following cell attachment, we treated the NT2Ns with APAP. For the MTT assays we used Nunc™ MicroWell™ 96-Well Microplates, whereas Corning® black-frame clear-bottom 96-well plates (Corning #3603) were used for all other experiments. For the MTT experiments, we coated the cell vessels with PLL (as described in the section on CGN preparation), in addition to using a secondary coating consisting of 320 ng/cm^2 fibronectin (ThermoFischer #33010018) applied using half of the intended seeding medium volume, into which the cells were seeded directly without removal of the coating solution. In the live-cell imaging (LCI) and ICC experiments we coated the vessels with PLL and Geltrex (as described in the section on CGN preparation). For the migration experiment we generated NT2N spheroids by re-seeding 10 mL of NT2N suspension into 100 mm low-adhesion dishes at 5 × 10^5 cells/mL which we incubated at 37 °C, 5% CO_2 overnight on a rotator. We then harvested and counted the spheroids in the same way as we did the CGN spheroids detailed above, and seeded them into PLL- and fibronectin-coated TPP® 96-well plates (Sigma-Aldrich #Z707910) plates using 1:1 mixture of conditioned and fresh defined medium, where the fresh half of the medium had been supplemented with 10 μM RA. After seeding, we incubated the spheroids at 37 °C, 5% CO_2 for 4 h before exchanging medium with fresh 1:1 conditioned/fresh defined medium with APAP treatment.

2.3. Treatment with APAP

We prepared 100 mM stock aliquots of APAP (Sigma-Aldrich #A7085) by dissolving the powder in MQ-water via vortexing at 37 °C, followed by sterile-filtration, aliquoting, and storage at −20 °C. Stocks were protected from light and never exposed to freeze-thaw cycles. We exposed the cells to a 4-step treatment-series ranging from 100 μM to 1600 μM APAP in defined medium. To equalize the dilution level of the medium resulting from the increasing volume of APAP stock added to increasing treatment concentrations, we supplemented the controls and all treatment concentrations below 1600 μM with the appropriate volumes of Milli-Q® water. For experiments lasting 72 h or less, we did not disturb the cells until termination of the experiment. For experiments lasting past 72 h, we performed a half-volume medium refresh every third day, where the freshly added media contained sample-appropriate APAP concentrations. To evaluate whether the effects of APAP on the protein levels of SPTBN1 were mediated by caspase-3, we co-exposed samples to APAP and an inhibitor of caspase-3 (Calbiochem #CAS 285570–60-7), dissolved in Milli-Q® water in stocks of 1 mM, and administered the inhibitor at a final concentration of 1 μM.

2.4. MTT viability assay

We used the colorimetric 3-(4,5-dimethylthiazol-2-yl)-2,5-diphenyltetrazolium bromide (MTT) assay, wherein cell reductive activity is used as a proxy for cell viability, to assess the cytotoxicity of APAP. Viable cells metabolize the yellow tetrazolium dye MTT into purple formazan, which is measured spectrophotometrically at 490/570 nm ex/em. Following seeding and treatment, we incubated the cells for 24, 48, and 72 h. To exclude the possibility of APAP influencing the assay results through chemical reduction of MTT, we replaced the treatment

medium with fresh defined medium supplemented with 0.5 μg/mL MTT (ThermoFischer #M6494), with the exception of 3 wells per plate which were used for background subtraction. Following MTT application we incubated the cells at 37 °C, 5% CO_2 for 2 h, after which we replaced the MTT-solution with 100 μL DMSO per well. We incubated the plates for another 30 min at 37 °C to dissolve the formazan crystals, then scanned them in a Clariostar Plus (BMG Labtech, Offenburg, Germany) plate-reader. We averaged the blank values obtained from the wells without MTT and subtracted the average blank value from the optical density values of the sample wells.

2.5. DNAq assay

We used an ICC-compatible, 4′,6-diamidino-2-phenylindole (DAPI)-based in-well method described by Ligasova & Koberna (Ligasová and Koberna, 2019) to quantify DNA in fixed samples. Following treatment and ICC, we washed the cells with PBS and re-fixed them in 70% ethanol for 10 min at room temperature, after which we airdried them for 30 min. We incubated the cells with 3 μM DAPI in 20 mM Tris-HCl with 150 mM NaCl (adjusted to pH 7) for 30 min on an agitator at room temperature. While protecting samples from light, we discarded the staining solution and washed the cells with a buffered solution composed of 2 mM $CuSO_4$, 0.5 M NaCl, 20 mM citrate, and 0.2% Tween (adjusted to pH 5) three times, 2 min per wash. We rinsed the cells with 20 mM Tris-HCl, 150 mM NaCl (adjusted to pH 7), then eluted the stained DNA using an elution solution composed of 2% SDS in 20 mM Tris-HCl (adjusted to pH 7) over the course of 15 min on an agitator at room temperature. Eluates were transferred into freshly washed Corning® 96-well 3603 plates and scanned using a Clariostar Plus microplate reader using the included DAPI filter (360–20/460–30 nm ex/em). DNA quantification readouts were used as cell viability assessment complementary and mechanistically orthogonal to the MTT assay data, in addition to being used as normalization factors for ICC data.

2.6. Live-cell imaging

We employed live-cell imaging (LCI) to evaluate the temporal effects of APAP on cell soma counts and neurite arborization dynamics. We seeded the cells into coated 96-well plates and treated them as detailed in the section on APAP treatment. Immediately following treatment, we placed the CGNs into IncuCyte ZOOM (EssenBioScience, Hertfordshire, UK) and the NT2Ns into IncuCyte S3 (EssenBioScience, Hertfordshire, UK) devices maintaining 37 °C and 5% CO_2, and scanned the plates, obtaining 4 images per well at 10× magnification, at 90-min intervals for a total of 72 h. We quantified neurite lengths and neurite branch points using a new analysis tool developed in-house, named Automated Neuronal Differentiation Analyzer (ANDA, manuscript in preparation). ANDA operates in conjunction with ImageJ (Schindelin et al., 2012) as an automated analysis pipeline for large sets of WEKA-segmented (Arganda-Carreras et al., 2017) time-series phase contrast images, capable of quantifying a variety of neuronal morphometrics (https://github.com/EskelandLab/ANDA). To validate the performance of ANDA, we analysed the CGN data set with the EssenBioScience IncuCyte ZOOM NeuroTrack module and compared the two sets of results (Fig. S1). The NeuroTrack module was trained using a set of analysis parameters optimized on the basis of a training set consisting of three images per time-point of untreated chicken cerebellar granule neurons from four different time-points: 6, 24, 48, and 72 h post-seeding (Table S1). For the WEKA-segmentation, a classification model was created for each cell type (Supplementary files), in both cases of which the training was performed on an image of an untreated sample at 72 h post-seeding. For assessment of migration by way of quantification of growth area coverage by cells migrating radially from spheroids, we used various image processing functions as well as the particle analysis function of ImageJ (macro in Table S2) on time-lapse phase contrast images of CGN and NT2N spheroids exposed to APAP. Samples of non-aggregated cell suspension were used as single-cell controls (SCC) and were included in all migration experiments in order to delineate migration from cell proliferation.

2.7. Immunocytochemistry

We performed ICC analysis on a series of protein targets to evaluate the effects of APAP on cellular levels of these proteins (Table S3). We seeded the cells into clear-bottom, black-frame 96-well plates and treated them as described in the sections on cell preparation and APAP treatment. Following treatment, we aspirated the treatment media and rinsed the cells with room-temperate phosphate-buffered saline (PBS), followed by fixation by application of −20 °C 99% methanol and incubation for 10 min at −20 °C. After fixation we added cold PBS directly into the methanol to prevent the cells from drying during the removal of methanol. We discarded the fixative solution and rinsed the cells 3 times with cold PBS. We blocked the cells overnight at 4 °C in blocking buffer (Tris-buffered saline (TBS) containing 0.05% Tween 20 (TBST) and 2.5% BSA). The following day we replaced the blocking buffer with blocking solution containing primary antibodies (mouse anti-SPTBN1 (BD Transduction Laboratories #612562) at 1:50 dilution, and rabbit anti-TUBB3 (Sigma-Aldrich #T2200) at 1:2000 dilution) and incubated the cells for 1 h on an orbital shaker at room temperature. We washed the cells 3 × 5 minutes with TBST, then incubated them in blocking buffer containing secondary antibodies (goat anti-rabbit Alexa 488 (Invitrogen #A-11070) and donkey anti-mouse Cy5 (Jackson ImmunoResearch #715–175-151), both at 1:1000 dilution) for 1 h on a shaker at room temperature. We washed the cells 3 × 5 minutes with TBST, rinsed with PBS, and maintained the samples in PBS at 4 °C until imaging (2–48 h). Prior to imaging, we rinsed the cells with PBS and replaced with fresh PBS in order to remove any solvated fluorophores. We included fluorescence controls of three types: sample wells incubated with no antibodies; sample wells incubated with primary antibodies only; sample wells incubated with secondary antibodies only. We imaged all ICC experiments at 20× magnification using an IncuCyte S3 (EssenBioScience, Essen BioScience, Ltd., Newark, UK) LCI platform, with exposure times of 550 milliseconds (green channel), and 950 milliseconds (red channel). We quantified the fluorescence intensities using a Clariostar Plus (BMG Labtech, Ortenberg, Germany) microplate reader using a dichromatic scan with the included 488 (488–14/535–30 nm ex/em) and Cy5 (610–30/675–50 nm ex/em) scan options. For quantification of punctate staining of TUBB3, we used particle analysis in ImageJ to count the number of high-intensity punctae in the fluorescence images obtained from the IncuCyte scans. For all ICC experiments except the 144- and 216-h NT2N experiments, as well as the procedure involving the caspase-inhibitor, we normalized the ICC fluorescence values and the TUBB3 counts to sample-corresponding DNAq values in order to account loss of cells between treatments. For the aforementioned exceptions, we normalized the SPTBN1 reads to sample-corresponding TUBB3 values, as we previously found that these covaried with DNAq reads.

2.8. Statistics

We used GraphPad Prism 8 (GraphPad Software, San Diego, CA, USA) to perform all statistical analyses. Analyses are reported as mean ± standard deviation (SD). All data were based on three repetitions per experiment, of which each repetition consisted of an independent population. For CGNs, we defined an independent population as cell culture that alone originated from a unique set of embryonic cerebella. For NT2Ns, the same definition applied for cell culture that was separately differentiated and which originated from undifferentiated NTERA2 cells that had been grown a minimum of three serial or parallel passages separated from culture of the same type, together constituting a minimum of one month of temporal separation from cell culture of the same type. Cell viability was assessed using the MTT and DNAq assays. MTT data for both CGNs and NT2Ns were based on six wells per treatment,

whereas DNAq was performed on 12 wells per treatment. LCI time-series data for quantification of neurite lengths and neurite branch points for CGNs were based on four wells per treatment, with four images taken per well per time point. Similar data for NT2Ns were based on twelve wells per treatment, with four images taken per well per time point. All migration analyses were performed on 12 wells per treatment, with four images taken er well per time point. SCC samples used in migration experiments were excluded from statistical analyses to avoid confounding bias in favour of treatment effect. ICC data for both CGNs and NT2Ns were based on three wells per treatment, with each well scanned once per orbital averaging level (0–6) at max number of flashes allowed per level, constituting a total of 570 flashes per well. Data on punctate staining of TUBB3 were based on three wells per treatment, with nine images taken per well. All data were evaluated using two-way ANOVA, with Dunnett's multiple comparisons test (MCT) used to determine significant difference between treatments and controls at $\alpha = 0.05$, from which lowest observed adverse effect levels (LOAELs), defined as lowest treatment concentrations showing significant difference from controls at any given time point, were derived. The experiment involving the caspase-inhibitor was evaluated using two-way ANOVA, with Dunnett's MCT comparing all group means at $\alpha = 0.05$.

3. Results

3.1. APAP reduces cell viability in both CGNs and NT2Ns

To evaluate the canonical view of APAP being a compound with little to no effect on cell viability at the employed concentrations, we exposed chicken CGNs and human NT2Ns to APAP in a 4-step concentration doubling gradient from 100 μM to 1600 μM for 24, 48, and 72 h. Using the MTT cell viability assay, we found a significant overall reduction of cell viability following exposure to APAP for the CGNs (two-way ANOVA: treatment effect $F_{(5,90)} = 6.027$, $p < 0.0001$; time effect $F_{(2,90)} = 238.3$, $p < 0.0001$, Fig. 1A) and the NT2Ns (two-way ANOVA: treatment effect $F_{(5,90)} = 18.06$, $p < 0.0001$; time effect $F_{(2,90)} = 76.7$, $p < 0.0001$, Fig. 1B). At 24 h post-exposure, no lowest-observed-adverse-effect level (LOAEL) was determined for either cell model, whereas at the 48-h mark we found a reduction in cell viability at 800 μM APAP in the NT2Ns (two-way ANOVA: adjusted $p = 0.0185$, Dunnett's MCT, ctrl vs P800 at 48 h), but no effect in the CGNs. At 72 h post-exposure, both cell models showed reductions in viability, with a LOAEL of 800 μM in the CGNs (two-way ANOVA: adjusted $p = 0.0018$, Dunnett's MCT, ctrl vs P800 at 72 h), and 200 μM in the NT2Ns (two-way ANOVA; adjusted $p = 0.0039$, Dunnett's MCT, ctrl vs P200 at 72 h). We also evaluated cell viability using the DNAq assay, where we found reductions in viability both for the CGNs (two-way ANOVA: treatment effect $F_{(5,198)} = 15.16$, $p < 0.0001$; time effect $F_{(2,198)} = 3.944$, $p = 0.209$, Fig. 1C) and the NT2Ns

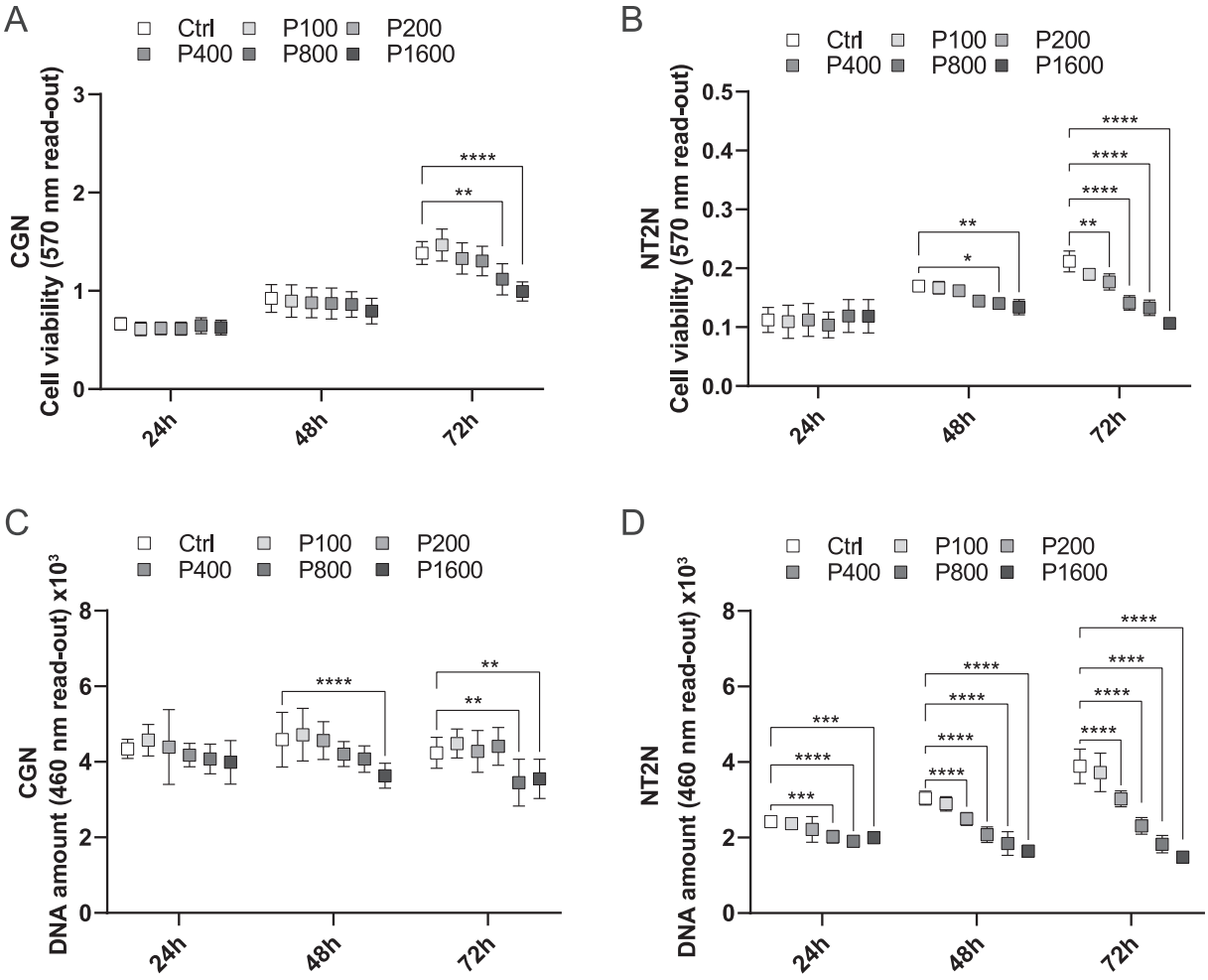

Fig. 1. The effects of APAP on cell viability in CGNs and NT2Ns. Cells were exposed to 100–1600 μM APAP (P100-P1600) for up to 72 h, followed by evaluation of cell viability using the MTT assay in (A) chicken CGNs and (B) human NT2Ns. Viability was also assessed using the DNAq assay in both the (C) CGNs and the (D) NT2Ns. Asterisks denote significance as determined by Dunnett's MCT, $\alpha = 0.05$, ctrl vs treatment, multiples = higher significance. All experiments were performed in biological triplicate, $n_{MTT} = 6$, $n_{DNAq} = 12$. All data are shown as mean ± SD.

(two-way ANOVA: treatment effect $F_{(5,198)} = 209.9$, $p < 0.0001$; time effect $F_{(2,198)} = 96.01$, $p < 0.0001$, Fig. 1D). After exposure for 24 h, no LOAEL was detected in the CGNs, whereas the LOAEL in the NT2Ns was determined to 400 μM (adjusted $p = 0.0004$, Dunnett's MCT, ctrl vs P400 at 24 h). At 48 h, the CGNs exhibited a LOAEL of 1600 μM (adjusted $p < 0.0001$, Dunnett's MCT, ctrl vs P1600 at 48 h), and the NT2Ns a LOAEL of 200 μM (adjusted $p < 0.0001$, Dunnett's MCT, ctrl vs P200 at 48 h). At 72 h post-exposure, the LOAEL in the CGNs had been reduced to 800 μM (adjusted $p = 0.0015$, Dunnett's MCT, ctrl vs P800 at 72 h), whereas the LOAEL of the NT2Ns remained at 200 μM (adjusted $p < 0.0001$,

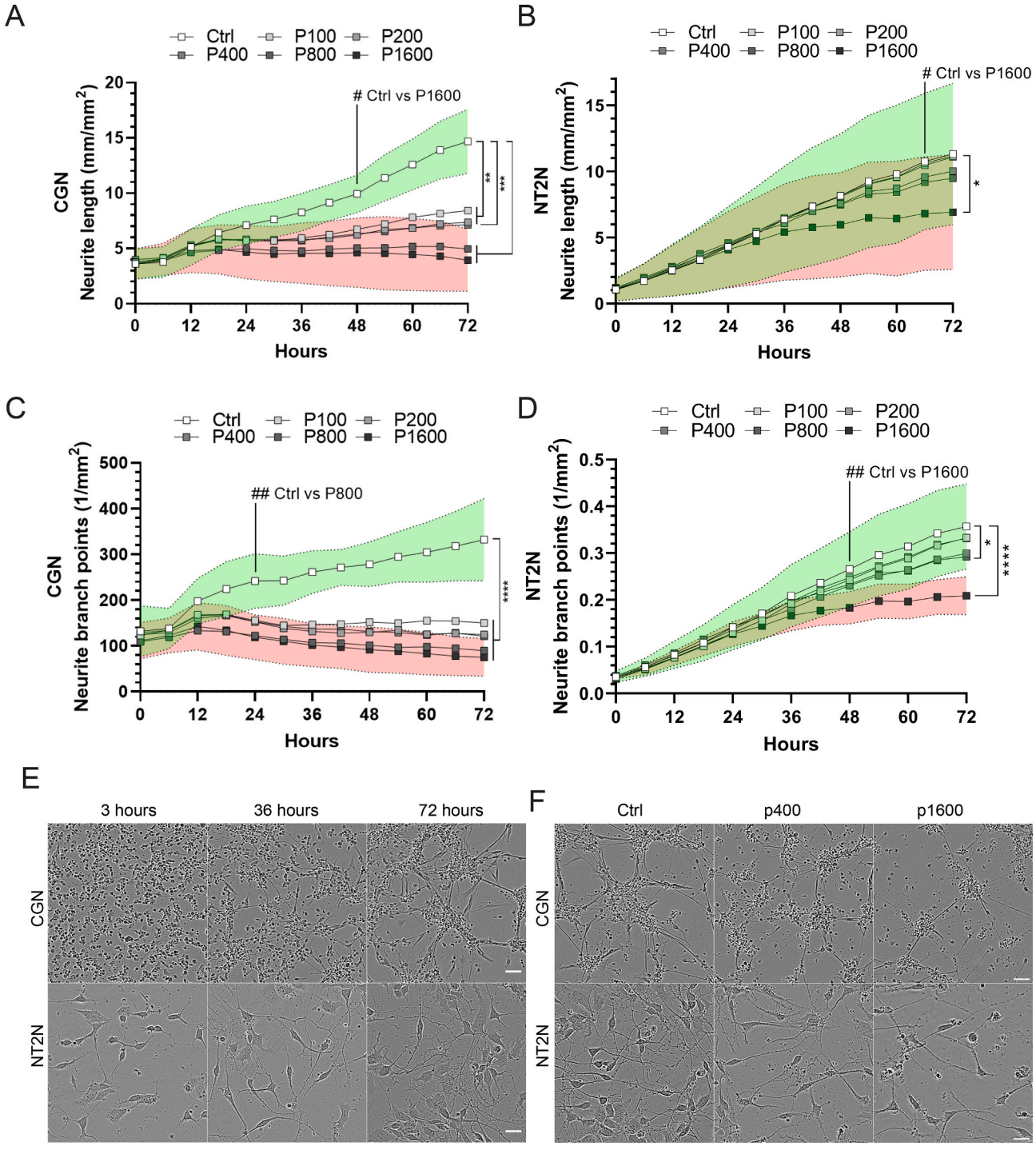

Fig. 2. The effects of APAP on neurite arborization in CGNs and NT2N. Cells were exposed to 100–1600 μM APAP (P100-P1600) for up to 72 h and imaged using LCI. The resultant phase contrast images were used to quantify the neurite lengths of (A) chicken CGNs and (B) human NT2Ns, as well as the neurite branch of points of (C) CGNs and (D) NT2Ns as determined by ANDA. (E) Representative phase contrast images of CGNs (top row) and NT2Ns (bottom row) from 3 h (first column), 36 h (middle column), and 72 h (last column). (F) Representative phase contrast images of CGNs (top row) and NT2Ns (bottom row) showing control samples (first column), and samples exposed to APAP at 400 μM (middle column), and 1600 μM (last column). Asterisks denote significance as determined by Dunnett's MCT, $\alpha = 0.05$, ctrl vs sample, multiples = higher significance. Hashes denote first LOAEL, multiples = higher significance. All experiments were performed in biological triplicate, $n_{CGN} = 4$, $n_{NT2N} = 12$, analysis based on 4 images per well. Images were taken at 10× magnification. Data are shown as means, with variance shown as ± SD for controls (green) and P1600 (red). (For interpretation of the references to colour in this figure legend, the reader is referred to the web version of this article.)

Dunnett's MCT, ctrl vs P200 at 72 h).

3.2. APAP reduces neurite arborization in both CGNs and NT2Ns

To delineate neurotoxic effects from viability-effecting cytotoxic effects, we assessed the effects of APAP on cellular neurite arborization via quantification of neurite lengths and neurite branch point numbers in LCI images. We used the EssenBioScience IncuCyte ZOOM NeuroTrack plugin to quantify neurite arborization in CGNs exposed to APAP. We observed concentration- and time-dependent reduction in both neurite lengths (two-way ANOVA: treatment effect $F_{(5,234)} = 15.07$, $p < 0.0001$; time effect $F_{(12,234)} = 4.76$, $p < 0.0001$, Fig. 2A) and neurite branch points (two-way ANOVA: treatment effect $F_{(5,234)} = 52.54$, $p < 0.0001$; time effect $F_{(12,234)} = 1.18$, $p = 0.29$, Fig. 2C) in CGNs exposed to APAP. First LOAEL in the CGN neurite lengths was detected at an APAP concentration of 1600 μM at 48 h (adjusted $p = 0.036$, Dunnett's MCT, ctrl vs 1600 μM at 48 h), whereas at 72 h post-exposure the LOAEL was as low as 100 uM APAP (adjusted $p = 0.0089$, Dunnett's MCT, ctrl vs 100 μM at 72 h). The CGN neurite branch points showed a first LOAEL at an APAP concentration of 800 μM at 24 h (adjusted $p = 0.0065$, Dunnett's

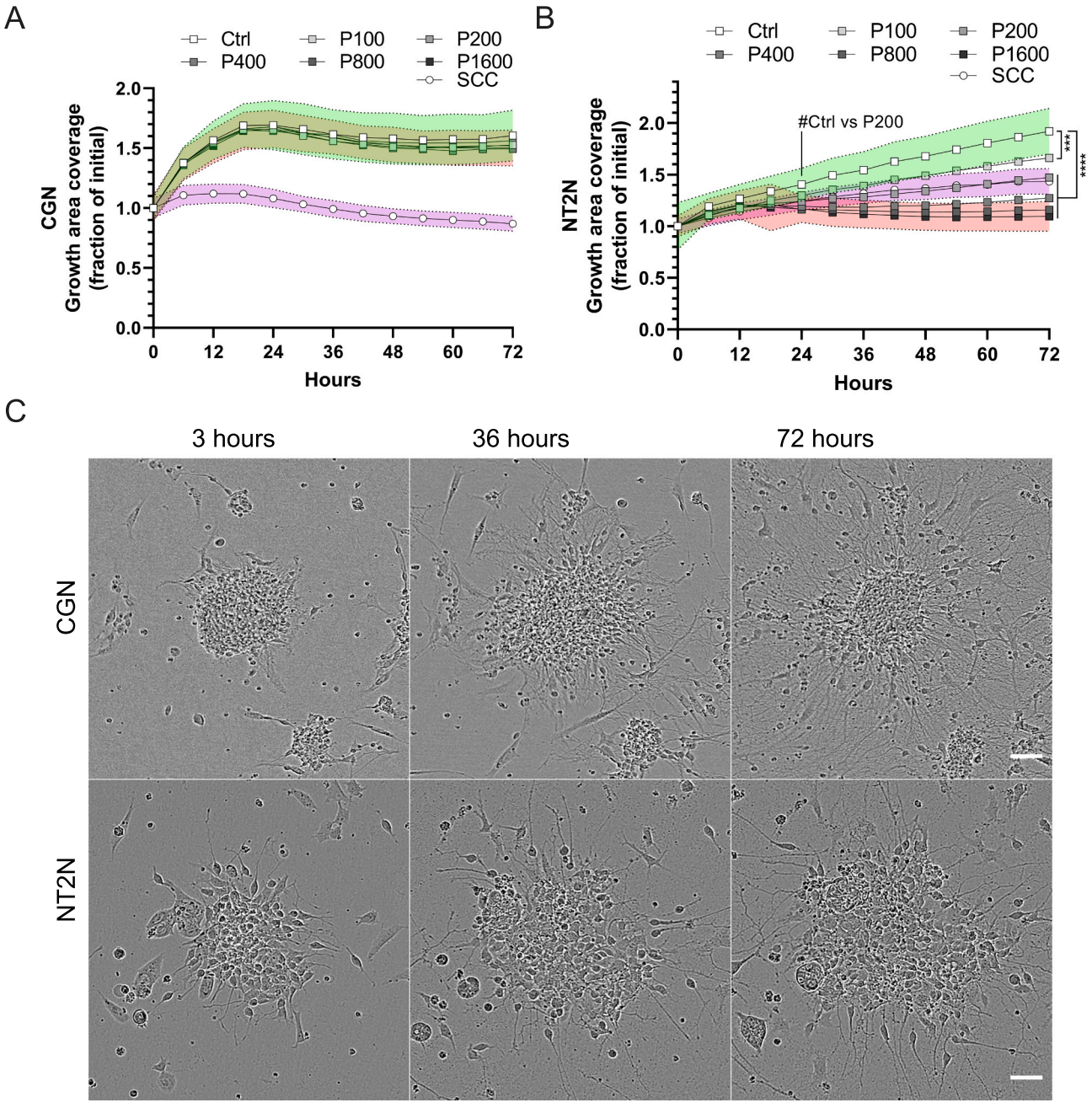

Fig. 3. The effects of APAP on migration in CGNs and NT2Ns. Cells were seeded as spheroids and exposed to 100–1600 μM APAP (P100-P1600) for up to 72 h and imaged using LCI. Untreated single-cell control (SCC) was included to distinguish migration from proliferation. The resultant phase contrast images were used to quantify migration by way of spheroid sprouting in (A) chicken CGNs and (B) human NT2Ns. (C) Representative phase contrast images of spheroids of CGNs (top row) and NT2Ns (bottom row) from 3 h (first column), 36 h (middle column), and 72 h (last column). SCCs were omitted from analyses. Asterisks denote significance as determined by Dunnett's MCT, α = 0.05, ctrl vs sample, multiples = higher significance. Hashes denote first LOAEL, multiples = higher significance. All experiments were performed in biological triplicate, $n = 12$, analysis based on 4 images per well. Images were taken at 10× magnification, scale bar = 50 μm. Data are shown as means, with variance shown as ± SD for controls (green), P1600 (red), and single-cell control (purple). (For interpretation of the references to colour in this figure legend, the reader is referred to the web version of this article.)

MCT, ctrl vs 800 μM at 24 h), which again was reduced to 100 μM APAP at 72 h post-exposure (adjusted $p < 0.0001$, Dunnett's MCT, ctrl vs 100 μM at 72 h). The difference between the means of the controls and the highest APAP concentrations (1600 μM) was found to be approximately 75% for both arborization metrics at termination of the experiment for the CGNs.

In the case of the NT2Ns, we also found concentration- and time-dependent reductions in both neurite lengths two-way ANOVA: treatment effect $F_{(5,858)} = 3.958$, $p = 0.0015$; time effect $F_{(12,858)} = 46.52$, $p < 0.0001$, (Fig. 2B) and neurite branch points (two-way ANOVA: treatment effect $F_{(5,858)} = 17.3$, $p < 0.0001$; time effect $F_{(12,858)} = 173.6$, $p < 0.0001$, Fig. 2D) following exposure to APAP. For the NT2N neurite lengths, the first LOAEL was determined to 1600 μM APAP at 66 h (adjusted $p = 0.0408$, Dunnett's MCT, ctrl vs 1600 μM at 66 h), where it remained to 72 h post-exposure (adjusted $p = 0.017$, Dunnett's MCT, ctrl vs 1600 μM at 72 h). The NT2N neurite branch points showed a first LOAEL of 1600 μM APAP at 48 h (adjusted $p = 0.0002$, Dunnett's MCT, ctrl vs 1600 μM at 48 h), and a 72-h LOAEL at an APAP concentration of 800 μM (adjusted $p = 0.0327$, Dunnett's MCT, ctrl vs 800 μM at 72 h). The means of the arborization metrics in the NT2Ns exhibited slightly lower effect sizes than their CGN counterparts, approximating control-relative reductions of 50% in the highest APAP concentrations at termination of experiment.

3.3. APAP reduces cell migration in NT2Ns but not in CGNs

To assess whether APAP exerted any effects on migration, we quantified the radial migration of cells from spheroids from time-series LCI using ImageJ to determine growth area coverage. While the CGNs showed a marginal concentration- and time-dependent response to treatment with APAP (two-way ANOVA: treatment effect $F_{(5,858)} = 2.365$, $p = 0.0382$; time effect $F_{(12,858)} = 73.87$, $p < 0.0001$, Fig. 3A and C, upper row), the NT2Ns exhibited a strong APAP-mediated concentration- and time-dependent decrease in migration (two-way ANOVA: treatment effect $F_{(5,858)} = 156.6$, $p < 0.0001$; time effect $F_{(12,858)} = 39.69$, $p < 0.0001$, Fig. 3B and C, bottom row). No LOAEL was determinate in the CGNs, whereas the first LOAEL in the NT2Ns was determined to 200 μM APAP already at 24 h (adjusted $p = 0.0457$, Dunnett's MCT, ctrl vs P200 at 24 h), and the 72-h LOAEL to 100 μM APAP (adjusted $p = 0.0004$, Dunnett's MCT, ctrl vs P100 at 72 h). In the CGNs the difference between the mean migration levels of the controls and the samples exposed to the highest APAP concentrations were negligible at termination of experiment at 72 h, whereas the highest APAP concentrations reduced mean migration levels by approximately half compared to the controls in the NT2Ns at the 72-h mark.

3.4. APAP specifically reduces protein levels of SPTBN1 in both CGNs and NT2Ns in a concentration-dependent manner, while having no effect on the levels of other neurodevelopmentally important proteins

To determine whether APAP perturbs the intracellular levels of proteins involved in neurodevelopmental processes or the maintenance of neuronal structure and function, we performed a series of ICC analyses on chicken CGNs and human NT2Ns at 72 and 120 h after exposure to APAP. We stained for proteins involved in neuronal differentiation: proliferating cell nuclear antigen (PCNA) for proliferation; paired box protein 6 (PAX6) and the neurofilament heavy chain (NFH) for neuronal differentiation; doublecortin (DCX) for migration; and for cytoskeleton proteins microtubule-associated protein 2 (MAP2), spectrin beta non-erythrocytic 1 (SPTBN1) and tubulin beta 3 class III (TUBB3, β3-tubulin) (Table S2). Additionally, glial fibrillary acidic protein (GFAP), which in early neurodevelopment is transiently expressed by neuroprogenitors in addition to being a marker of glial populations, was included to assess any potential effects of APAP on gliotoxicity. We found that exposure to APAP strongly and specifically reduced the protein levels of SPTBN1 in a concentration- and time-dependent manner in both CGNs (two-way ANOVA: treatment effect $F_{(5,24)} = 22.08$, $p < 0.0001$; time effect $F_{(1,24)} = 1.365$, $p = 0.2542$, Fig. 4A and B, control top row) and NT2Ns (two-way ANOVA: treatment effect $F_{(5,24)} = 6.383$, $p = 0.0007$; time effect $F_{(1,24)} = 3.242$, $p = 0.0843$, Fig. 4A and B, control bottom row). In the CGNs, the first LOAEL was determined to 400 μM APAP at 72 h (adjusted $p = 0.0447$, Dunnett's MCT, ctrl vs 400 μM at 72 h), whereas the 120-h LOAEL was determined to 800 μM APAP (adjusted $p = 0.0065$, Dunnett's MCT, ctrl vs 800 μM at 120 h). In the NT2Ns, the first LOAEL was determined to 1600 μM APAP at 120 h (adjusted $p = 0.0009$, Dunnett's MCT, ctrl vs 1600 μM at 120 h). In both cell models, the mean levels of SPTBN1 were reduced by approximately 50% in response to 1600 μM APAP over 72 h, and by approximately 75% over the course of 120 h, relative to their respective controls. To evaluate whether the APAP-mediated reduction of SPTBN1-levels constituted a threshold phenomenon, we also exposed both cell models to subtherapeutic APAP concentration equivalents ranging from 25 to 100 μM, finding no difference from control at any concentration for any time-point (Fig. S2). Additionally, to assess whether the observed reductions in SPTBN1 levels were mediated by caspase-3, we exposed NT2Ns to 1600 μM APAP ±1 μM of an inhibitor of caspase-3 for 72 and 120 h, the results of which indicated no involvement of caspase-3 (Fig. S3). We observed no changes in protein levels of PCNA, PAX6, DCX, GFAP, NFH, MAP2, or TUBB3 following exposure of either cell model to 100–1600 μM APAP for 72 h (Fig. S4).

3.5. APAP increases punctate aggregation of TUBB3 in both CGNs and NT2Ns

While we found no effects of APAP on the protein levels of TUBB3 in either cell model, visual inspection revealed increasing levels of punctate aggregation of TUBB3 in both CGNs and NT2Ns exposed to APAP (Fig. 5B). An APAP-mediated increase in punctate aggregation was not observed for any other protein we stained for (Fig. S5). We quantified the high-intensity punctae and found an overall increase in the number of TUBB3-stained punctae following exposure to increasing levels of APAP in both CGNs (two-way ANOVA: treatment effect $F_{(5,24)} = 4.704$, $p = 0.0039$; time effect $F_{(1,24)} = 0.03852$, $p = 0.846$) and NT2Ns two-way ANOVA: treatment effect $F_{(5,24)} = 10.64$, $p < 0.0001$; time effect $F_{(1,24)} = 4.866$, $p = 0.0372$, Fig. 5A). For the CGNs, LOAELs remained indeterminate, whereas for the NT2Ns, the first LOAEL was determined to 1600 μM at 72 h in the NT2Ns (adjusted $p = 0.0107$, Dunnett's MCT, ctrl vs 1600 μM at 72 h), as was the 120-h mark LOAEL (adjusted $p = 0.0005$, Dunnett's MCT, ctrl vs 1600 μM at 120 h). The increase in the mean number of punctae between the controls and the highest APAP concentrations was found to be approximately 60% for both time-points in the CGNs, whereas the number of punctae approximately doubled over both treatment times in the NT2Ns.

4. Discussion

In this study, we demonstrated that in vitro exposure of embryonic chicken CGNs and neuronally differentiating human NT2Ns to increasing concentrations of APAP led to concentration- and time-dependent increases in negative outcomes in a series of neurodevelopmentally important metrics. Most results were qualitatively similar between the animal-derived and human-derived neurodevelopmental models, suggesting that the observed effects of APAP might be species-independent. To minimize potential confounding effects that could arise from the use of organic compounds as solvents, we used Milli-Q® water to dissolve APAP. The aqueous solubility of APAP has previously been reported to be 132 mM at 37 °C (Hunt and Dunford, 1977), on the grounds of which we prepared 100 mM stock solutions. Stocks were prepared by sequential vortexing and heating in a 37 °C water bath until no remaining particulate matter could visibly be detected, at which point solution was sterile filtered and aliquoted. We stored the stocks at −20 °C, and upon thawing performed

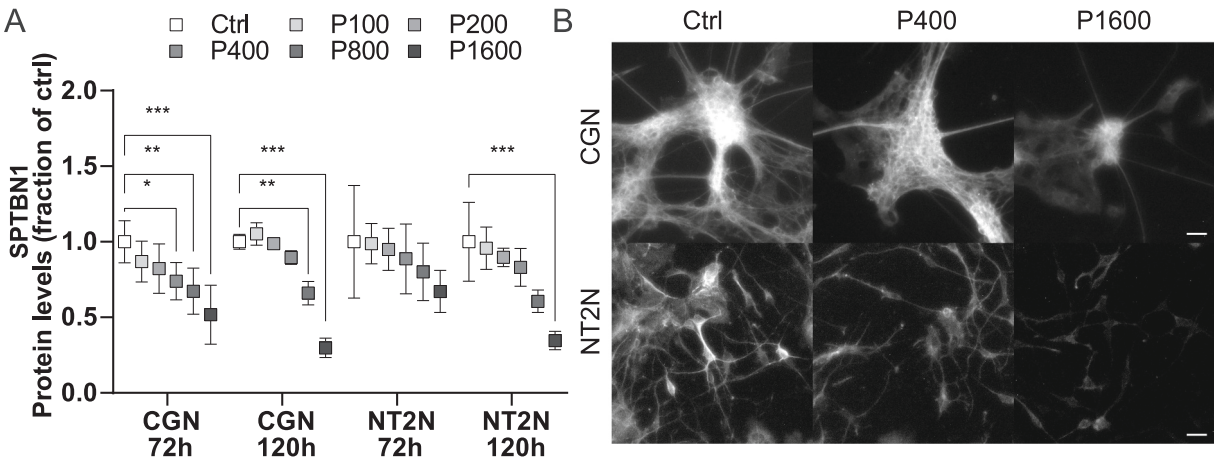

Fig. 4. The effects of APAP on protein levels of SPTBN1. Cells were exposed to 100–1600 μM APAP (P100-P1600) for 72 and 120 h, then fixed, stained for SPTBN1, and (A) quantified using a plate-reader. (B) Fluorescent images of SPTBN1 in control samples of CGNs (top row) and NT2Ns (bottom row), exposed to increasing concentrations of APAP. Asterisks denote significance as determined by Dunnett's MCT, $\alpha = 0.05$, ctrl vs sample, multiples = higher significance. All experiments were performed in biological triplicate, $n = 3$. Fluorescence reads were normalized to DNAq reads, then to their respective untreated controls. Images were taken at 20× magnification, scale bar = 50 μm. All data are shown as mean ± SD.

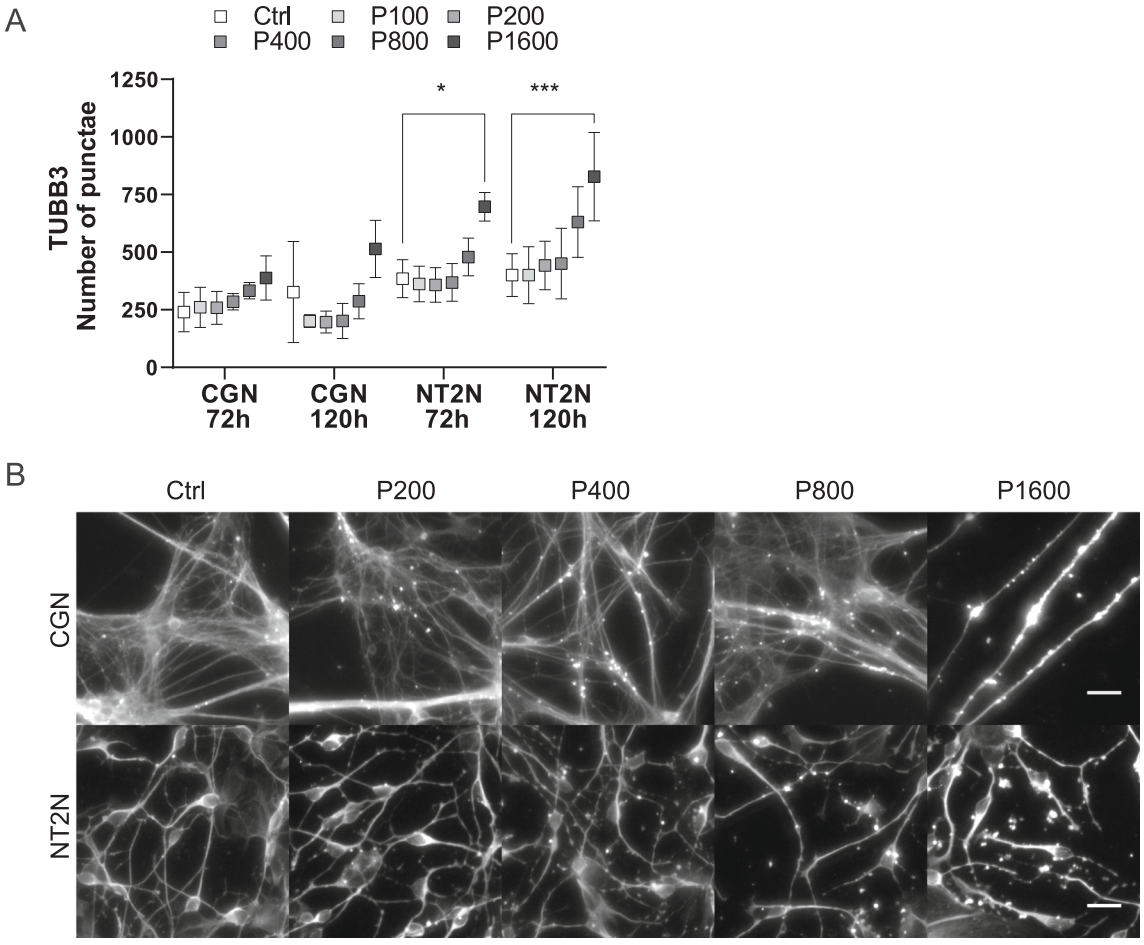

Fig. 5. The effects of APAP on the punctate aggregation of TUBB3. Cells were exposed to 100–1600 μM APAP (P100–1600) for 72 and 120 h. Following fixation and staining, cells were imaged and (A) the numbers of TUBB3-stained aggregates were quantified using ImageJ. (B) ICC of TUBB3 in CGNs (upper panels) and NT2Ns (lower panels), treated with increasing concentrations of APAP. Asterisks denote significance as determined by Dunnett's MCT, $\alpha = 0.05$, ctrl vs sample, multiples = higher significance. All experiments were performed in biological triplicate, n = 3, analysis based on 9 images per well. Images were taken at 20× magnification, scale bar = 50 μM. Punctate counts were normalized to DNAq reads. All data are shown as mean ± SD.

aforementioned heating and vortexing routine until no visible particulate matter remained. Thawed stocks were not filtered. All stock and working APAP solutions were protected from light as much as possible during stock and sample preparation and were used immediately and never reused. A saturated aqueous solution of APAP has a pH of 6 (WHO, 1990), and previous investigations into the heat stability of APAP in aqueous solutions report a degradation rate of approximately 7% per year at 35 °C in aqueous solution at pH 6 (Gilpin and Zhou, 2004). We thus assume the potential physiochemical degradation of APAP during stock and sample preparation, as well as over the course of incubation to be negligible, suggesting all observed results to be biochemical in nature.

Evaluation of cell viability by the MTT assay showed that exposure to APAP concentration- and time-dependently reduced cell viability in both cell models relative to their respective untreated controls at the same time-points. While the effects of treatment with APAP on cell viability were qualitatively similar, the NT2Ns exhibited a steeper concentration-dependent decline in viability at 48 and 72 h compared to the CGNs, suggesting a higher degree of vulnerability to perturbation by APAP. The MTT data also showed that there was a time-dependent increase in viability across all samples, with even the most negatively affected APAP-exposed samples never exhibiting viabilities below the levels of their respective 24-h controls. ICC quantification of the protein levels of PCNA in samples exposed to APAP over 72 h showed no control-relative changes in response to APAP at any concentration (Fig. S4A), suggesting that the viability-reducing effects of APAP proceed independently of proliferation. The DNAq assay yielded results similar to that of the MTT assay, showing concentration- and time-dependent reductions in DNA amounts in response to APAP exposure. In contrast to the MTT assay, however, the DNAq assay did not show a time-dependent overall increase in viability in the CGN samples. Since the CGN culture medium was supplemented with the mitotic inhibitor AraC, large-scale proliferation would have been inhibited irrespective of any potential proliferation-inhibiting effects APAP might harbour. As the MTT assay measures viability by proxy of metabolism, the discrepancy might be attributable to the MTT assay detecting proliferation-independent increases in cellular metabolic rates as energy-intensive processes such as neuritogenesis (Trigo et al., 2019) and the rise of a neuronal network with signaling capacity (Berndt and Holzhütter, 2013; Harris and Attwell, 2012) evolved over time. Similar to the MTT results, the DNAq showed a steeper concentration-dependent loss of cell viability in response to exposure to APAP in the NT2Ns compared to the CGNs. In contrast to the CGNs, the overall time-dependent increase in cell viability observed in the MTT assay was corroborated by results from the DNAq assay in the NT2Ns. As the culture medium of the NT2Ns was not supplemented with AraC, proliferation is the most likely explanation to this time-dependent increase in viability. However, since none of the APAP-treated NT2N samples showed any control-relative changes in PCNA levels (Fig. S4A), we conclude the APAP-mediated reductions in viabilities for both cell models to proceed by means independent of changes in proliferation. The effects of APAP on the viabilities of neuronal progenitors, primary neurons, and neuronal and glial cell lines have been assessed by different studies, and our results generally fall in line with these findings. Exposures to APAP at concentrations up to around 1 mM for 12 to 24 h indicate little to no effect on cell viability (Xie and Harvey, 1993; Mannerström et al., 2006; Tripathy and Grammas, 2009; Schultz et al., 2012; Posadas et al., 2010; Oksuz et al., 2021), whereas exposure times over 48 h result in both concentration- and time-dependent reductions in cell viabilities at APAP concentrations above 500 μM (Oksuz et al., 2021; Posadas et al., 2012; Buzanska et al., 2009; Kobolak et al., 2020). We show that longer and increase in concentration of APAP decreases cell viability.

We also found that exposure to APAP resulted in concentration- and time-dependent reductions in both neurite lengths and neurite branch points in both cell models. Both arborization metrics exhibited much larger effect-sizes and earlier first LOAELs in the CGNs compared to the NT2Ns. This effect is most likely due to the CGNs developing a mature neuronal network much faster than the NT2Ns, which again presumably reflects the difference in gestational developmental time between the organisms from which the cells were derived, where embryonic development in chickens is complete within 21 days, contrasted with 40 weeks for humans (Bjørnstad et al., 2015). The in vitro development of a mature, signaling-capable neuronal network in the NT2Ns requires another 2–4 weeks of treatment with a cocktail of mitotic inhibitors (Hartley et al., 1999; Schwartz et al., 2005; Hill et al., 2012). Considering the higher sensitivity of the NT2Ns to the viability-reducing effects of APAP, and taking into account the relatively similar effect sizes between the two cell models in the case of the highest APAP concentrations at the 72-h mark, it seems reasonable to posit that the control-relative reductions of both arborization metrics in the APAP-treated samples would be as pronounced, if not higher, in the NT2Ns than in the CGNs if the experimental time-window for the NT2Ns was expanded to reflect the difference in maturation-rate. Previous studies have found no effects of APAP in concentrations ranging from 10 nM to 10 μM on numbers of neurites or branch points in treatment periods lasting 14 days in human neuronal progenitors (Wu et al., 2016), nor at a concentration of 100 μM over the course of 4 days in rat PC12 cells (Radio et al., 2008). However, investigations in developing zebrafish have found that 5-day full-body exposures to APAP at concentrations as low as 6.6 μM result in detectable reductions in axonal lengths, with a concentration of 165 μM resulting in a 75% reduction in axonal lengths (Zhang and Gong, 2013).

Our investigation into the effects of APAP on migration provided the only stark difference in response between the two cell models, as exposure to APAP strongly concentration- and time-dependently reduced the migration levels of the NT2Ns, while eliciting a barely detectable reduction in migration in the CGNs. The most parsimonious explanation for the discrepancy might be found in the difference in clustering behaviour between the two cell types, as single-cell seed-out of CGNs readily begin aggregating into clusters over the course of a few days (Fig. 2E, top row), whereas the NT2Ns exhibit no clustering behaviour (Fig. 2E, bottom row) until they reach a later maturation stage, achieved by treating them with mitotic inhibitors for at least 7 days in monolayer format (Goodfellow et al., 2011). From the quantification of migration in the CGNs it is apparent that following an initial migrational spurt lasting from seeding and up until the 18-h mark, the growth area coverage plateaus towards the 24-h mark, after which it recedes slightly, then stabilizes to a steady state. As these results are consistent with a natural clustering predisposition, the explanation of the difference in response to APAP between the two cell models might be that the CGNs are simply a less suitable cell type for modelling migration by way of spheroid sprouting. In support of a mechanistic explanation for the lack of a migrational response to APAP, ICC staining of CGNs for the migration-related protein DCX also showed no effect in response to APAP (Fig. S4C). While the NT2Ns showed a clear concentration- and time-dependent reduction in migration in response to exposure to APAP, ICC staining following APAP treatment showed no changes in levels of DCX in these cells either, rendering the mechanistic underpinnings of the effect inconclusive. Although previous research has found no changes in cytoarchitecture or expression levels of the migration-related protein reelin in mice exposed to APAP (Philippot et al., 2021), the APAP metabolite AM404 has been found to inhibit migration in neuroblastoma cells (Caballero et al., 2015), raising the possibility that the observed APAP-mediated reduction in migration in NT2Ns is specific to cell lines of carcinoma origin.

When staining fixed cells for protein targets we found a strong and specific concentration- and time-dependent reduction in the cytoskeletal protein SPTBN1 in both cell models, an effect not observed in protein levels of PCNA, PAX6, DCX, GFAP, NFH, MAP2, or TUBB3. This effect was qualitatively similar in both cell models, suggesting that unlike the observed effects of APAP on neurite arborization, this effect was independent of the rate of neuronal maturation. While we found no changes in levels of TUBB3 in CGNs, we noticed a minor concentration-

dependent trend towards increasing levels of TUBB3 in the NT2Ns (Fig. S4M). Exposure to high concentrations of APAP is known to cause cellular oxidative stress (Du et al., 2016; Ramachandran and Jaeschke, 2019), and NTERA2 cells are known to express TUBB3 when undergoing oxidative stress (González-Burguera et al., 2016; Hu et al., 2018), suggesting that the slight NT2N-specific increase in TUBB3 observed at higher APAP concentrations might be due to this particular idiosyncratic response of the NTERA2 cells. In addition to this, we also discovered a concentration-dependent increase in the number of high-intensity punctae in the TUBB3 staining in APAP-exposed cells of both models. These punctae are reminiscent of neuritic beading observed in in vitro neurons exposed to excitotoxic treatments, as well in in vivo cases of some neurodegenerative disorders (Tan et al., 2007; Sadleir et al., 2016). While we observed this effect in both cell models, the effect was drastically stronger in the NT2Ns compared to the CGNs, again suggesting that the NT2Ns are more sensitive to APAP-mediated toxicity.

To facilitate the drastic cellular morphological changes taking place during neuritogenesis, cargo is continuously transported bidirectionally by motor proteins on microtubule. Ablation of SPTBN1 has previously been shown to markedly reduce bidirectional transport along neurites (Lorenzo et al., 2019), leading us to hypothesize that the observed APAP-mediated reduction in SPTBN1 might be the driving factor behind the coinciding reduction in neuronal arborization, as well as the increase in punctate aggregation of TUBB3 by way of disruption of the transport system along the neurites. SPTBN1 has previously noted to undergo caspase-3/7-mediated proteolysis in response to APAP-exposure in hepatocytes (Baek et al., 2016), but we found no indication of involvement of caspase-3 when co-exposed NT2Ns to APAP and a caspase-3-inhibitor (Fig. S3). While both cell models exhibited qualitatively similar responses to exposure to APAP, the human NT2Ns exhibited a stronger response in all metrics except in the reduction of arborization, which we expect to be explicable by the dramatically slower rate of development and maturation of the neuronal network in the case of the NT2Ns. Taken together our findings demonstrate that exposure to APAP in in vitro human and chicken models undergoing early neurodevelopment concentration- and time-dependently perturbs neuritogenesis, resulting in reduced overall levels of neurite arborization, and that this effect coincides with reductions in the protein levels of SPTBN1 and the disruption of the structural integrity of TUBB3.

5. Conclusion

In conclusion, we have addressed the effects of in vitro exposure of embryonic chicken CGNs and neuronally differentiating human NT2Ns to APAP ranging from subtherapeutic to hepatotoxic concentrations. Exposure of differentiating neurons to APAP led to similar concentration- and time-dependent negative effects on cell viability and neuritogenesis in both cell models. Further studies are needed to assess whether these observed modes of action of APAP can describe potential risk factors leading neurodevelopmental disorders including ADHD during in off-springs of mothers with long-term use of APAP.

Funding

University of Oslo PhD Grant (NAL); PharmaTox Strategic Research Initiative was supported by Faculty of Mathematics and Natural Sciences, University of Oslo.

CRediT authorship contribution statement

Nils-Anders Labba: Conceptualization, Methodology, Investigation, Formal analysis, Writing – original draft, Writing – review & editing. **Hallvard Austin Wæhler:** Software, Investigation, Resources, Writing – original draft, Writing – review & editing. **Nora Houdaifi:** Investigation. **Denis Zosen:** Investigation. **Fred Haugen:** Conceptualization, Resources. **Ragnhild Elisabeth Paulsen:** Conceptualization, Resources, Project administration, Supervision, Writing – original draft, Writing – review & editing. **Mussie Ghezu Hadera:** Conceptualization, Investigation. **Ragnhild Eskeland:** Conceptualization, Resources, Project administration, Supervision, Writing – original draft, Writing – review & editing.

Declaration of Competing Interest

The authors declare that there are no conflicts of interest.

Acknowledgements

The authors extend their gratitude to: Athina Samara of the Department of Women's and Children's Health, Karolinska Institute, Sweden, for providing antibodies and insightful discussion on both theory and methodology; Mona Gaarder and Beata Mohebi of the Department of Pharmacy, University of Oslo for invaluable support in the laboratory; Merete Thune Wiiger and Mariana Vincenti of the Norwegian Radium Hospital for sharing analytic equipment and accommodating the idiosyncratic work-hours of the first author in spite of a global pandemic; Else Marit Inderberg of Oslo Cancer Cluster for sharing analytic equipment; and Johanna Samulin-Erdem of The National Institute of Occupational Health, Norway for sharing analytic equipment. Some of the informatic analysis was performed at saga super computing resources (Project NN9632K) provided by UNINETT Sigma2—the National Infrastructure for High Performance Computing and Data Storage in Norway. We thank CanCell, UiO for use of computing infrastructure.

Appendix A. Supplementary data

Supplementary data to this article can be found online at https://doi.org/10.1016/j.taap.2022.116130.

References

Anderson, B.J., Holford, N.H.G., Woollard, G.A., Chan, P.L.S., 1998. Paracetamol plasma and cerebrospinal fluid pharmacokinetics in children. Br. J. Clin. Pharmacol. 46 (3), 237–243. https://doi.org/10.1046/j.1365-2125.1998.00780.x.

Arganda-Carreras, I., et al., 2017. Trainable Weka segmentation: a machine learning tool for microscopy pixel classification. Bioinformatics 33 (15), 2424–2426. https://doi.org/10.1093/bioinformatics/btx180.

Baek, H.J., et al., 2016. Caspase-3/7-mediated cleavage of β2-spectrin is required for acetaminophen-induced liver damage. Int. J. Biol. Sci. 12 (2), 172–183. https://doi.org/10.7150/ijbs.13420.

Bakulski, K.M., Halladay, A., Hu, V.W., Mill, J., Fallin, M.D., 2016. Epigenetic research in neuropsychiatric disorders: the 'tissue issue. Curr. Behav. Neurosci. Rep. 3 (3), 264–274. https://doi.org/10.4135/9781452234144.n117.

Bannwarth, B., et al., 1992. Plasma and cerebrospinal fluid concentrations of paracetamol after a single intravenous dose of propacetamol. Br. J. Clin. Pharmacol. 34 (1), 79–81. https://doi.org/10.1111/j.1365-2125.1992.tb04112.x.

Beare, R., et al., 2017. Altered structural connectivity in ADHD: a network based analysis. Brain Imaging Behav. 11 (3), 846–858. https://doi.org/10.1007/s11682-016-9559-9.

Berndt, N., Holzhütter, H.G., 2013. The high energy demand of neuronal cells caused by passive leak currents is not a waste of energy. Cell Biochem. Biophys. 67 (2), 527–535. https://doi.org/10.1007/s12013-013-9538-3.

Bjørnstad, S., Peter, L., Austdal, E., Roald, B., Glover, J.C., Paulsen, R.E., 2015. Minireviews cracking the egg: potential of the developing chicken as a model system for nonclinical safety studies of pharmaceuticals. J. Pharmacol. Exp. Ther. 355, 386–396. https://doi.org/10.1124/jpet.115.227025.

Blecharz-Klin, K., et al., 2015a. Developmental exposure to paracetamol causes biochemical alterations in medulla oblongata. Environ. Toxicol. Pharmacol. 40 (2), 369–374. https://doi.org/10.1016/j.etap.2015.07.001.

Blecharz-Klin, K., et al., 2015b. Effect of prenatal and early life paracetamol exposure on the level of neurotransmitters in rats-focus on the spinal cord. Int. J. Dev. Neurosci. 47, 133–139. https://doi.org/10.1016/j.ijdevneu.2015.09.002.

Blecharz-Klin, K., et al., 2017. Paracetamol – effect of early exposure on neurotransmission, spatial memory and motor performance in rats. Behav. Brain Res. 323, 162–171. https://doi.org/10.1016/j.bbr.2017.01.051.

Blecharz-Klin, K., et al., 2018. Early paracetamol exposure decreases brain-derived neurotrophic factor (BDNF) in striatum and affects social behaviour and exploration in rats. Pharmacol. Biochem. Behav. https://doi.org/10.1016/j.pbb.2018.03.004.

Blecharz-Klin, K., Wawer, A., Pyrzanowska, J., Piechal, A., Jawna-Zboińska, K., Widy-Tyszkiewicz, E., 2019. Hypothalamus – response to early paracetamol exposure in

male rats offspring. Int. J. Dev. Neurosci. 76 (January), 1–5. https://doi.org/10.1016/j.ijdevneu.2019.05.004.
Brandlistuen, R.E., Ystrom, E., Nulman, I., Koren, G., Nordeng, H., 2013. Prenatal paracetamol exposure and child neurodevelopment: a sibling-controlled cohort study. Int. J. Epidemiol. 42 (6), 1702–1713. https://doi.org/10.1093/ije/dyt183.
Buzanska, L., et al., 2009. A human stem cell-based model for identifying adverse effects of organic and inorganic chemicals on the developing nervous system. Stem Cells 27 (10), 2591–2601. https://doi.org/10.1002/stem.179.
Caballero, F.J., et al., 2015. AM404 inhibits NFAT and NF-κB signaling pathways and impairs migration and invasiveness of neuroblastoma cells. Eur. J. Pharmacol. 746, 221–232. https://doi.org/10.1016/j.ejphar.2014.11.023.
Carmona, S., et al., 2005. Global and regional gray matter reductions in ADHD: a voxel-based morphometric study. Neurosci. Lett. 389 (2), 88–93. https://doi.org/10.1016/j.neulet.2005.07.020.
Cousin, M.A., et al., 2021. Pathogenic SPTBN1 variants cause an autosomal dominant neurodevelopmental syndrome. Nat. Genet. 53 (7), 1006–1021. https://doi.org/10.1038/s41588-021-00886-z.
de Fays, L., et al., 2015. Use of paracetamol during pregnancy and child neurological development. Dev. Med. Child Neurol. https://doi.org/10.1111/dmcn.12745.
De Felice, A., Ricceri, L., Venerosi, A., Chiarotti, F., Calamandrei, G., 2015. Multifactorial origin of neurodevelopmental disorders: approaches to understanding complex etiologies. Toxics 3 (1), 89–129. https://doi.org/10.3390/toxics3010089.
Du, K., Ramachandran, A., Jaeschke, H., 2016. Oxidative stress during acetaminophen hepatotoxicity: sources, pathophysiological role and therapeutic potential. Redox Biol. 10 (September), 148–156. https://doi.org/10.1016/j.redox.2016.10.001.
Forrest, J.A.H., Clements, J.A., Prescott, L.F., 1982. Clinical pharmacokinetics of paracetamol. Clin. Pharmacokinet. 7 (2), 93–107. https://doi.org/10.2165/00003088-198207020-00001.
Froomes, P.R.A., Morgan, D.J., Smallwood, R.A., Angus, P.W., 1999. Comparative effects of oxygen supplementation on theophylline and acetaminophen clearance in human cirrhosis. Gastroenterology 116 (4), 915–920. https://doi.org/10.1016/S0016-5085(99)70075-2.
Gilpin, R.K., Zhou, W., 2004. Studies of the thermal degradation of acetaminophen using a conventional HPLC approach and electrospray ionization-mass spectrometry. J. Chromatogr. Sci. 42 (1), 15–20. https://doi.org/10.1093/chromsci/42.1.15.
González-Burguera, I., et al., 2016. Highly efficient generation of glutamatergic/cholinergic NT2-derived postmitotic human neurons by short-term treatment with the nucleoside analogue cytosine β-d-arabinofuranoside. Stem Cell Res. 16 (2), 541–551. https://doi.org/10.1016/j.scr.2016.02.038.
Goodfellow, C.E., Graham, S.E., Dragunow, M., Glass, M., 2011. Characterization of NTera2/D1 cells as a model system for the investigation of cannabinoid function in human neurons and astrocytes. J. Neurosci. Res. 89 (10), 1685–1697. https://doi.org/10.1002/jnr.22692.
Graham, G.G., Day, R.O., Milligan, M.K., Ziegler, J.B., Kettle, A.J., 1999. Current concepts of the actions of paracetamol (acetaminophen) and NSAIDS. Inflammopharmacology 7 (3), 255–263. https://doi.org/10.1007/s10787-999-0008-x.
Harris, J.J., Attwell, D., 2012. The energetics of CNS white matter. J. Neurosci. 32 (1), 356–371. https://doi.org/10.1523/JNEUROSCI.3430-11.2012.
Hartley, R.S., Margulis, M., Fishman, P.S., Lee, V.M.Y., Tang, C.M., 1999. Functional synapses are formed between human NTera2 (NT2N, hNT) neurons grown on astrocytes. J. Comp. Neurol. 407 (1), 1–10. https://doi.org/10.1002/(SICI)1096-9861(19990428)407:1<1::AID-CNE1>3.0.CO;2-Z.
Hill, E.J., Jiménez-González, C., Tarczyluk, M., Nagel, D.A., Coleman, M.D., Parri, H.R., 2012. NT2 derived neuronal and astrocytic network signalling. PLoS One 7 (5), 1–10. https://doi.org/10.1371/journal.pone.0036098.
Hu, Q., et al., 2018. Oxidative stress promotes exit from the stem cell state and spontaneous neuronal differentiation. Oncotarget 9 (3), 4223–4238. https://doi.org/10.18632/oncotarget.23786.
Hunt, C.A., Dunford, P.R., 1977. Acetaminophen. J. Am. Pharm. Assoc. 17 (8), 517–521. https://doi.org/10.1016/S0003-0465(16)34428-7.
Ji, Y., et al., 2020. Association of cord plasma biomarkers of in utero acetaminophen exposure with risk of attention-deficit/hyperactivity disorder and autism spectrum disorder in childhood. JAMA Psychiatry 77 (2), 180–189. https://doi.org/10.1001/jamapsychiatry.2019.3259.
Kim, Y.S., Woo, J., Lee, C.J., Yoon, B.E., 2017. Decreased glial GABA and tonic inhibition in cerebellum of mouse model for attention-deficit/ hyperactivity disorder (ADHD). Exp. Neurobiol. 26 (4), 206–212. https://doi.org/10.5607/en.2017.26.4.206.
Kobolak, J., et al., 2020. Human induced pluripotent stem cell-derived 3D-neurospheres are suitable for neurotoxicity screening. Cells 9 (5). https://doi.org/10.3390/cells9051122.
Kondziolka, D., et al., 2005. Neurotransplantation for patients with subcortical motor stroke: a phase 2 randomized trial. J. Neurosurg. 103 (1), 38–45. https://doi.org/10.3171/jns.2005.103.1.0038.
Kumpulainen, E., Kokki, H., Halonen, T., Heikkinen, M., Savolainen, J., Laisalmi, M., 2007. Paracetamol (acetaminophen) penetrates readily into the cerebrospinal fluid of children after intravenous administration. Pediatrics 119 (4), 766–771. https://doi.org/10.1542/peds.2006-3378.
Lee, H.J., Lee, K., Im, H., 2012. α-Synuclein modulates neurite outgrowth by interacting with SPTBN1. Biochem. Biophys. Res. Commun. 424 (3), 497–502. https://doi.org/10.1016/j.bbrc.2012.06.143.
Liew, Z., Ritz, B., Rebordosa, C., Lee, P.C., Olsen, J., 2014. Acetaminophen use during pregnancy, behavioral problems, and hyperkinetic disorders. JAMA Pediatr. 168 (4), 313–320. https://doi.org/10.1001/jamapediatrics.2013.4914.
Ligasová, A., Koberna, K., 2019. Quantification of fixed adherent cells using a strong enhancer of the fluorescence of DNA dyes. Sci. Rep. 9 (1), 1–12. https://doi.org/10.1038/s41598-019-45217-9.
Lorenzo, D.N., Badea, A., Zhou, R., Mohler, P.J., Zhuang, X., Bennett, V., 2019. βII-spectrin promotes mouse brain connectivity through stabilizing axonal plasma membranes and enabling axonal organelle transport. Proc. Natl. Acad. Sci. U. S. A. 116 (31), 15686–15695. https://doi.org/10.1073/pnas.1820649116.
Machnicka, B., et al., 2014. Spectrins: a structural platform for stabilization and activation of membrane channels, receptors and transporters. Biochim. Biophys. Acta Biomembr. 1838 (2), 620–634. https://doi.org/10.1016/j.bbamem.2013.05.002.
Mannerström, M., Toimela, T., Ylikomi, T., Tähti, H., 2006. The combined use of human neural and liver cell lines and mouse hepatocytes improves the predictability of the neurotoxicity of selected drugs. Toxicol. Lett. 165 (2), 195–202. https://doi.org/10.1016/j.toxlet.2006.04.002.
Marks, D.J.B., et al., 2017. Outcomes from massive paracetamol overdose: a retrospective observational study. Br. J. Clin. Pharmacol. 83 (6), 1263–1272. https://doi.org/10.1111/bcp.13214.
Martine Hoogman, P., 2017. Subcortical brain volume differences of participants with ADHD across the lifespan: an ENIGMA collaboration. Lancet Psychiatry 4 (4), 310–319. https://doi.org/10.1016/S2215-0366(17)30049-4.Subcortical.
McElhatton, P.R., Sullivan, F.M., Volans, G.N., 1997. Paracetamol overdose in pregnancy analysis of the outcomes of 300 cases referred to the teratology information service. Reprod. Toxicol. 11 (1), 85–94. https://doi.org/10.1016/S0890-6238(96)00200-6.
Meltzer, C.C., et al., 2001. Serial [18F]fluorodeoxyglucose positron emission tomography after human neuronal implantation for stroke. Neurosurgery 49 (3), 586–592. https://doi.org/10.1227/00006123-200109000-00011.
Mostofsky, S.H., Cooper, K.L., Kates, W.R., Denckla, M.B., Kaufmann, W.E., 2002. Smaller prefrontal and premotor volumes in boys with attention-deficit/hyperactivity disorder. Biol. Psychiatry 52 (8), 785–794. https://doi.org/10.1016/S0006-3223(02)01412-9.
Mueller, B.K., Ledig, M.M., Wahl, S., 2000. From the growth cone surface to the cytoskeleton: one journey, many paths. J. Neurobiol. 44 (2), 184–193. https://doi.org/10.1002/1097-4695(200008)44:2<184::AID-NEU8>3.0.CO;2-N.
Nelson, P.T., et al., 2002. Clonal human (hNT) neuron grafts for stroke therapy: neuropathology in a patient 27 months after implantation. Am. J. Pathol. 160 (4), 1201–1206. https://doi.org/10.1016/S0002-9440(10)62546-1.
Nitsche, J.F., et al., 2017. Transplacental passage of acetaminophen in term pregnancy. Am. J. Perinatol. 34 (6), 541–543. https://doi.org/10.1055/s-0036-1593845.
Oksuz, E., Gorgisen, G., Ozdemir, H., Gulacar, I.M., Oto, G., 2021. Effect of paracetamol in the proliferation of glioblastoma cell line: the role of apoptosis, COX-2 and cyclin B expressions. Turk. Neurosurg. 31 (1), 46–50. https://doi.org/10.5137/1019-5149.JTN.27866-19.7.
Philippot, G., Hellsten, S.V., Viberg, H., Fredriksson, R., 2021. Evaluation of the dentate gyrus in adult mice exposed to acetaminophen (paracetamol) on postnatal day 10. Int. J. Dev. Neurosci. 81 (1), 91–97. https://doi.org/10.1002/jdn.10079.
Pleasure, S.J., Page, C., Lee, V.M.Y., 1992. Pure, postmitotic, polarized human neurons derived from NTera 2 cells provide a system for expressing exogenous proteins in terminally differentiated neurons. J. Neurosci. 12 (5), 1802–1815. https://doi.org/10.1523/jneurosci.12-05-01802.1992.
Posadas, I., Santos, P., Blanco, A., Muñoz-Fernández, M., Ceña, V., 2010. Acetaminophen induces apoptosis in rat cortical neurons. PLoS One 5 (12), 1–14. https://doi.org/10.1371/journal.pone.0015360.
Posadas, I., Santos, P., Ceña, V., 2012. Acetaminophen induces human neuroblastoma cell death through NFKB activation. PLoS One 7 (11). https://doi.org/10.1371/journal.pone.0050160.
Radio, N.M., Breier, J.M., Shafer, T.J., Mundy, W.R., 2008. Assessmentof chemical effects on neurite outgrowth in PC12 cells using high content screening. Toxicol. Sci. 105 (1), 106–118. https://doi.org/10.1093/toxsci/kfn114.
Ramachandran, A., Jaeschke, H., 2019. Acetaminophen Hepatotoxicity: A Mitochondrial Perspective, , 1st ed.vol. 85. Elsevier Inc. https://doi.org/10.1016/bs.apha.2019.01.007
Sachana, M., et al., 2019. International regulatory and scientific effort for improved developmental neurotoxicity testing. Toxicol. Sci. 167 (1), 172–189. https://doi.org/10.1093/toxsci/kfy211.
Sadleir, K.R., Kandalepas, P.C., Buggia-Prévot, V., Nicholson, D.A., Thinakaran, G., Vassar, R., 2016. Presynaptic dystrophic neurites surrounding amyloid plaques are sites of microtubule disruption, BACE1 elevation, and increased Aβ generation in Alzheimer's disease. Acta Neuropathol. 132 (2), 235–256. https://doi.org/10.1007/s00401-016-1558-9.
Satterstrom, F.K., et al., 2019. Autism spectrum disorder (ASD) and attention-deficit/hyperactivity disorder (ADHD) have a similar burden of rare protein-truncating variants. Nat. Neurosci. 22 (12), 1961–1965. https://doi.org/10.1038/s41593-019-0527-8.Autism.
Schindelin, J., et al., 2012. Fiji: an open-source platform for biological-image analysis. Nat. Methods 9 (7), 676–682. https://doi.org/10.1038/nmeth.2019.
Schiødt, F.V., Ott, P., Christensen, E., Bondesen, S., 2002. The value of plasma acetaminophen half-life in antidote-treated acetaminophen overdosage. Clin. Pharmacol. Ther. 71 (4), 221–225. https://doi.org/10.1067/mcp.2002.121857.
Schultz, S., Desilva, M., Gu, T.T., Qiang, M., Whang, K., 2012. Effects of the analgesic acetaminophen (paracetamol) and its para-aminophenol metabolite on viability of mouse-cultured cortical neurons. Basic Clin. Pharmacol. Toxicol. 110 (2), 141–144. https://doi.org/10.1111/j.1742-7843.2011.00767.x.
Schultz, S., Gould, G.G., Antonucci, N., Brigida, A.L., Siniscalco, D., 2021. Endocannabinoid system dysregulation from acetaminophen use may lead to autism

spectrum disorder: could cannabinoid treatment be efficacious? Molecules 26 (7). https://doi.org/10.3390/molecules26071845.
Schwartz, C.M., et al., 2005. NTera2: a model system to study dopaminergic differentiation of human embryonic stem cells. Stem Cells Dev. 14 (5), 517–534. https://doi.org/10.1089/scd.2005.14.517.
Serra, M., Leite, S.B., Brito, C., Costa, J., Carrondo, M.J.T., Alves, P.M., 2007. Novel culture strategy for human stem cell proliferation and neuronal differentiation. J. Neurosci. Res. 85 (16), 3557–3566. Dec. https://doi.org/10.1002/jnr.21451.
Sidlauskaite, J., Caeyenberghs, K., Sonuga-Barke, E., Roeyers, H., Wiersema, J.R., 2015. Whole-brain structural topology in adult attention-deficit/hyperactivity disorder: preserved global - disturbed local network organization. NeuroImage Clin. 9, 506–512. https://doi.org/10.1016/j.nicl.2015.10.001.
Sikorski, A.F., Sangerman, J., Goodman, S.R., Critz, S.D., 2000. Spectrin (βSpIIΣ1) is an essential component of synaptic transmission. Brain Res. 852 (1), 161–166. https://doi.org/10.1016/S0006-8993(99)02253-2.
Stergiakouli, E., Thapar, A., Smith, G.D., 2016. Association of acetaminophen use during pregnancy with behavioral problems in childhood: evidence against confounding. JAMA Pediatr. 170 (10), 964–970. https://doi.org/10.1001/jamapediatrics.2016.1775.
Stern, M., Gierse, A., Tan, S., Bicker, G., 2014. Human Ntera2 cells as a predictive in vitro test system for developmental neurotoxicity. Arch. Toxicol. https://doi.org/10.1007/s00204-013-1098-1.
Stoodley, Catherine J., 2016. The cerebellum and neurodevelopmental disorders. Cerebellum 15, 34–37. https://doi.org/10.1007/s12311-015-0715-3.The.
Susuki, K., et al., 2011. Schwann cell spectrins modulate peripheral nerve myelination. Proc. Natl. Acad. Sci. U. S. A. 108 (19), 8009–8014. https://doi.org/10.1073/pnas.1019600108.
Tan, Z., et al., 2007. Mutant ubiquitin found in Alzheimer's disease causes neuritic beading of mitochondria in association with neuronal degeneration. Cell Death Differ. 14 (10), 1721–1732. https://doi.org/10.1038/sj.cdd.4402180.
Thompson, J.M.D., Waldie, K.E., Wall, C.R., Murphy, R., Mitchell, E.A., 2014. Associations between acetaminophen use during pregnancy and ADHD symptoms measured at ages 7 and 11 years. PLoS One 9 (9). https://doi.org/10.1371/journal.pone.0108210.
Tian, N., et al., 2012. Lipid raft-dependent endocytosis of close homolog of adhesion molecule L1 (CHL1) promotes neuritogenesis. J. Biol. Chem. 287 (53), 44447–44463. https://doi.org/10.1074/jbc.M112.394973.
Toda, K., 2017. Is acetaminophen safe in pregnancy? Scand J Pain 17, 445–446. https://doi.org/10.1016/j.sjpain.2017.09.007.
Tovo-Rodrigues, L., et al., 2018. Is intrauterine exposure to acetaminophen associated with emotional and hyperactivity problems during childhood? Findings from the 2004 Pelotas birth cohort. BMC Psychiatry 18 (1), 1–11. https://doi.org/10.1186/s12888-018-1942-1.
Trettin, A., et al., 2014. Effects of paracetamol on NOS, COX, and CYP activity and on oxidative stress in healthy male subjects, rat hepatocytes, and recombinant NOS. Oxidative Med. Cell. Longev. 3, 2014. https://doi.org/10.1155/2014/212576.
Trigo, D., Goncalves, M.B., Corcoran, J.P.T., 2019. The regulation of mitochondrial dynamics in neurite outgrowth by retinoic acid receptor β signaling. FASEB J. 33 (6), 7225–7235. https://doi.org/10.1096/fj.201802097R.
Tripathy, D., Grammas, P., 2009. Acetaminophen inhibits neuronal inflammation and protects neurons from oxidative stress. J. Neuroinflammation 6, 1–9. https://doi.org/10.1186/1742-2094-6-10.
Viberg, H., Eriksson, P., Gordh, T., Fredriksson, A., 2014. Paracetamol (acetaminophen) administration during neonatal brain development affects cognitive function and alters its analgesic and anxiolytic response in adult male mice. Toxicol. Sci. 138 (1), 139–147. https://doi.org/10.1093/toxsci/kft329.
WHO, 1990. IARC working group on the evaluation of carcinogenic risks to humans. Pharmaceutical drugs. In: IARC Monographs on the Evaluation of the Carcinogenic Risks to Humans, No. 50. https://www.ncbi.nlm.nih.gov/books/NBK526213/.
World Health Organization, 2008. The global burden of disease 2004. Glob. Burd. Dis. 2004 Updat. 146.
Wu, X., Majumder, A., Webb, R., Stice, S.L., 2016. High content imaging quantification of multiple in vitro human neurogenesis events after neurotoxin exposure. BMC Pharmacol. Toxicol. 17 (1), 1–15. https://doi.org/10.1186/s40360-016-0107-4.
Xie, K., Harvey, A.L., 1993. Evaluation of nerve cell toxicity in vitro by electrophysiological and biochemical methods. Toxicol. in Vitro 7 (3), 275–279. https://doi.org/10.1016/0887-2333(93)90012-T.
Xu, K., Zhong, G., Zhuang, X., 2013. Actin, spectrin, and associated proteins form a periodic cytoskeletal structure in axons. Science 339 (6118), 452–456. https://doi.org/10.1126/science.1232251.
Ye, H., Nelson, L.J., Del Moral, M.G., Martínez-Naves, E., Cubero, F.J., 2018. Dissecting the molecular pathophysiology of drug-induced liver injury. World J. Gastroenterol. 24 (13), 1373–1385. https://doi.org/10.3748/wjg.v24.i13.1373.
Ystrom, E., et al., 2017. Prenatal exposure to acetaminophen and risk of ADHD. Pediatrics 140 (5). https://doi.org/10.1542/peds.2016-3840.
Zhang, X., Gong, Z., 2013. Fluorescent transgenic zebrafish Tg(nkx2.2a:mEGFP) provides a highly sensitive monitoring tool for neurotoxins. PLoS One 8 (2). https://doi.org/10.1371/journal.pone.0055474.
Zhong, G., et al., 2014. Developmental mechanism of the periodic membrane skeleton in axons. Elife 3, 1–21. https://doi.org/10.7554/eLife.04581.